Numerical simulation of unsteady flow in natural and thermosolutal convection using boundary-fitted coordinate system

J.M. Zhan

*Department of Applied Mechanics and Engineering,
Zhongshan University, Guangzhou, People's Republic of China*

Y.S. Li

*Department of Civil and Structural Engineering,
The Hong Kong Polytechnic University, Hong Kong,
People's Republic of China*

Abstract *A numerical scheme is proposed to solve double-diffusive problems using a boundary-fitted coordinate system to introduce finer grids in the boundary layer regions and an accurate high-order difference method. Numerical stability is improved by using fourth-order accurate upwind-biased differences to approximate the convection terms. The other terms in the governing differential equations are discretized using fourth-order central difference. To demonstrate the versatility of the boundary-fitted coordinate system, natural convection in an eccentric annulus is first simulated. The numerical results are consistent with the experimental results by Kuehn and Goldstein and better than the numerical results by Projahn et al. for eccentric cases. Secondly, the symmetry breaking and overturning states in thermohaline-driven flows in a two-dimensional rectangular cavity are simulated first to validate the numerical scheme. The numerical results agree well with those by Dijkstra and Molemaker and Quon and Ghil. Finally, the effect of the Lewis number on the flow system is investigated in detail. Depending on the value of the Lewis number, the flow pattern is either stable and symmetric, periodic and oscillatory, or unsymmetric and random.*

Nomenclature

A = area of computational domain

D = cylinder diameter

E_m = kinetic energy $\left[= \frac{1}{A} \iint_A \frac{1}{2}(u^2 + \nu^2)\, \mathrm{d}x\, \mathrm{d}y\right]$

g = gravitational acceleration

H = width of cavity

$\bar{k}_{eq}$ = average equivalent conductivity

L = difference of radius $[= (D_o - D_i)/2]$

Le = Lewis number κ_T/κ_S

p = nondimensional pressure

Pr = Prandtl number, ν/κ_T

Q_s = spatial structure of the surface salt-flux

R_S = solutal Rayleigh number
R_T = thermal Rayleigh number
R_ρ = buoyancy ratio, R_S/R_T
S = nondimensional salinity
T = nondimensional temperature
u, v = nondimensional velocity components
x, y = nondimensional coordinates
ε = distance inner cylinder is moved from concentric position
κ = diffusivity
ν = kinematic viscosity
ξ, η = boundary-fitted coordinates

ρ = dimensional density
δ = strength of the surface salt flux
ψ = nondimensional stream function
ω = nondimensional vorticity

Subscripts
H = horizontal
i = inner cylinder
o = outer cylinder
S = salt
T = heat
V = vertical

Introduction

Thermosolutal convection has been receiving much attention over the past three decades because of its occurrence in many transport processes in both natural and industrial flow systems, such as drying processes, crystal growth techniques, climatic conditioning of rooms, cooling of nuclear reactors, solar collectors, atmospheric flows, and ocean circulations.

A number of studies on double-diffusive problems have been carried out. Lee and Hyun (1990) numerically studied the convection in a rectangular cavity with counteracting, horizontal temperature and concentration gradients. It was found that a multi-layered flow structure occurred when the value of the buoyancy ratio (the ratio of the solutal Rayleigh number to the thermal Rayleigh number) was moderate. Quon and Ghil (1992) studied the spontaneous, abrupt changes in thermohaline circulation using a two-dimensional Boussinesq fluid in a rectangular container. It was found that the symmetric circulation was replaced by an asymmetric flow when the specified symmetric salinity surface condition was changed to an equivalent symmetric salt-flux condition. The extent of asymmetry depends on the magnitude of the thermal Rayleigh number and the strength of the salinity flux. The physical mechanism of the bifurcation from symmetric to asymmetric states was also outlined. Quon and Ghil (1995) subsequently found that, for an enclosure of very small height-to-length aspect ratio, the system undergoes a second bifurcation from asymmetric steady states to stable oscillatory solutions when the salt-flux strength was sufficiently large. From a detailed study of the bifurcation structure that Dijkstra and Molemaker (1997) concluded the occurrence of oscillations was quite sensitive to the shape of the prescribed surface salt flux.

Several numerical methods have been used to study the convection problems. Heinrich (1984) and Nishimura and Kawamura (1992) used the finite element method. Lee and Hyun (1991) used a finite difference method to simulate the experiments of Chen *et al.* (1971). Nishimura and Kunitsugu (2000) studied the time-dependent double-diffusive convection in a rectangular

enclosure to clarify mechanism of layer merging in a salt-stratified system using the Chebyshev collocation method. The numerical modelling of double-diffusive problems is difficult because of the existence of large velocity, temperature and salinity gradients in the boundary layer, making the computational cost prohibitive. For high speed flows, an extensive amount of computational effort is required even for single-diffusive problems which have been employed as test cases to validate numerical schemes.

The finite-element method, with the flexibility of a variable mesh, is more versatile than the finite-difference method in handling geometrically complex domains, but is inferior to the finite-difference method in terms of computer programming effort and numerical stability. The boundary-fitted coordinate system (Thompson, 1980; Thompson *et al.*, 1974), which has the advantage of both the geometric flexibility of the finite-element method and the simplicity of the finite-difference method, has gained popularity in the solution of fluid flow problems. Some techniques for automatic mesh generation, which facilitates the application of the physical boundary conditions, were proposed by Li *et al.* (1998). In this paper, a high-order difference scheme is proposed for resolving the oscillatory flow phenomenon in double-diffusive problems under the boundary-fitted coordinate system. The proposed scheme is both accurate and stable. The natural convection in an eccentric annulus and multiple equilibria in thermohaline-driven flows in a two-dimensional rectangular cavity are simulated to validate the numerical scheme. Then the effect of the Lewis number on the thermohaline flow system was investigated in detail.

Governing equations and boundary conditions

We consider natural convection between eccentric cylinders and thermosolutal convection in a rectangular cavity. At high Rayleigh numbers, the effects of the boundary layers are significant and hence fine computational grids have been used. The governing equations are the two-dimensional, time-dependent Navier-Stokes equations with the Boussinesq assumptions incorporated. The differential equations, after nondimensionalizing the velocity components u and v, pressure p, temperature T and salinity S using characteristic scales L, κ_T/L, ΔT, and ΔS for length, velocity, temperature and salinity, respectively, are as follows using standard notation.

$$\frac{\partial u}{\partial x} + \frac{\partial v}{\partial y} = 0 \tag{1}$$

$$\frac{\partial u}{\partial t} + u\frac{\partial u}{\partial x} + v\frac{\partial u}{\partial y} = -\frac{\partial p}{\partial x} + \mathrm{Pr}\nabla^2 u \tag{2}$$

$$\frac{\partial v}{\partial t} + u\frac{\partial v}{\partial x} + v\frac{\partial v}{\partial y} = -\frac{\partial p}{\partial y} + \mathrm{Pr}\nabla^2 v + \mathrm{Pr}(\mathrm{R_T}T - \mathrm{R_S}S) \tag{3}$$

$$\frac{\partial T}{\partial t} + u\frac{\partial T}{\partial x} + v\frac{\partial T}{\partial y} = T_{xx} + T_{yy} \tag{4}$$

$$\frac{\partial S}{\partial t} + u\frac{\partial S}{\partial x} + v\frac{\partial S}{\partial y} = \frac{1}{\text{Le}}(S_{xx} + S_{yy}) \tag{5}$$

In order to minimize the number of grid points to reduce computational cost, the boundary-fitted coordinate system is employed to introduce finer grids to resolve better flow in the boundary layers. The one-to-one relation $\xi = \xi(x, y)$, $\eta = \eta(x, y)$ between the physical plane and the transformed regular plane can be established by solving numerical elliptic equations (Li et $al.$, 1998; Thompson, 1980; Thompson et $al.$, 1974). Introducing the stream function

$$u = \frac{\partial \psi}{\partial y}, \quad v = -\frac{\partial \psi}{\partial x}$$

and vorticity

$$\omega = \frac{\partial v}{\partial x} - \frac{\partial u}{\partial y}$$

equations (1)-(5) under the boundary-fitted coordinate system become

$$-\frac{1}{J^2}(\alpha\psi_{\xi\xi} - 2\beta\psi_{\xi\eta} + \gamma\psi_{\eta\eta} + \sigma\psi_\eta + \tau\psi_\xi) = \omega \tag{6}$$

$$\frac{\partial \omega}{\partial t} + \frac{1}{J}\left(\frac{\partial \psi}{\partial \eta}\frac{\partial \omega}{\partial \xi} - \frac{\partial \psi}{\partial \xi}\frac{\partial \omega}{\partial \eta}\right) = \frac{\text{Pr}}{J^2}(\alpha\omega_{\xi\xi} - 2\beta\omega_{\xi\eta} + \gamma\omega_{\eta\eta} + \sigma\omega_\eta + \tau\omega_\xi)$$
$$+ \text{Pr}\cdot\text{R}_\text{T}\left(y_\eta\frac{\partial(T - R_\rho S)}{\partial \xi} - y_\xi\frac{\partial(T - R_\rho S)}{\partial \eta}\right)\Big/J \tag{7}$$

$$\frac{\partial T}{\partial t} + \frac{1}{J}\left(\frac{\partial \psi}{\partial \eta}\frac{\partial T}{\partial \xi} - \frac{\partial \psi}{\partial \xi}\frac{\partial T}{\partial \eta}\right) = \frac{1}{J^2}(\alpha T_{\xi\xi} - 2\beta T_{\xi\eta} + \gamma T_{\eta\eta} + \sigma T_\eta + \tau T_\xi) \tag{8}$$

$$\frac{\partial S}{\partial t} + \frac{1}{J}\left(\frac{\partial \psi}{\partial \eta}\frac{\partial S}{\partial \xi} - \frac{\partial \psi}{\partial \xi}\frac{\partial S}{\partial \eta}\right) = \frac{1}{\text{Le}J^2}(\alpha S_{\xi\xi} - 2\beta S_{\xi\eta} + \gamma S_{\eta\eta} + \sigma S_\eta + \tau S_\xi) \tag{9}$$

where $\alpha = x_\eta^2 + y_\eta^2$, $\beta = x_\xi x_\eta + y_\xi y_\eta$, $\gamma = x_\xi^2 + y_\xi^2$, $J = x_\xi y_\eta - y_\xi x_\eta$, $\sigma = J^2 Q$, $\tau = J^2 P$ and P and Q are the coordinate control functions (Thompson et $al.$, 1974), which may be chosen to concentrate the coordinate lines in certain parts of the domain where high variations of a given property were expected.

Boundary conditions are

$$\psi = 0 \quad \text{on all solid boundaries} \tag{10}$$

$$T = T_{\text{h}} \quad \text{on high-temperature wall} \tag{11}$$

$$T = T_{\text{l}} \quad \text{on low-temperature wall} \tag{12}$$

$$\frac{\partial T}{\partial n} = 0 \quad \text{on insulated wall} \tag{13}$$

$$\frac{\partial S}{\partial n} = 0 \quad \text{on impervious wall} \tag{14}$$

If there are heat and salt fluxes through a boundary, such as on ocean surface, the usual mixed boundary conditions were given by Dijkstra and Molemaker (1997):

$$\psi = \omega = 0, \quad T = T_{\text{s}}(x), \quad \frac{\partial S}{\partial z} = \delta Q_{\text{s}}(x) \tag{15}$$

where the function $T_{\text{s}}(x)$ is a prescribed temperature distribution along the boundary. The parameter δ measures the strength of the surface salt-flux and $Q_{\text{s}}(x)$ represents its spatial structure. When the surface integral of this function is zero, the total salt content is conserved.

For an insulated or impervious boundary, the physical boundary condition is $\partial f / \partial n = 0$ ($f = T$ or S). It will be more convenient to treat the boundary condition if the transformed coordinate lines intersect, which were arranged perpendicular to the wall (Li *et al.*, 1998). For such cases, the following boundary condition on the walls can be used for grid generation,

$$(\vec{r}_{\text{w}} - \vec{r}_{\text{w}-1}) \cdot \vec{\tau}_{\text{w}} = 0, \tag{16}$$

where $\vec{\tau}_{\text{w}}$ is the unit tangential vector on the wall, $\vec{r}_{\text{w}}$ is the position vector of a grid point on the wall and $\vec{r}_{\text{w}-1}$ is an adjacent grid point in the same coordinate line perpendicular to the wall. The insulated or impervious boundary condition $\partial f / \partial n = 0$ can be simplified to

$$\frac{\partial f}{\partial \xi} = 0, \quad \text{for} \quad \eta = \text{const}$$

$$\tag{17}$$

$$\frac{\partial f}{\partial \eta} = 0, \quad \text{for} \quad \xi = \text{const}$$

In this paper, all coordinate lines intersecting with the walls were arranged perpendicular to ease the application of the boundary conditions.

High-order accurate finite difference method

In this paper, equation (6) is solved using the over-relaxation method. Convergence is assumed to be achieved when the absolute values of the difference of ψ between the successive iteration steps are less than 10^{-8}. Although the time steps Δt used in the test cases given below were very small, the absolute values of the differences of ψ between the successive steps at the early stage of iteration are not very small because the values of the Rayleigh number used are large, which are in the range of 10^3-10^4. A smaller value of 10^{-9} have been used as the critical value for convergence and the results are the same as those using 10^{-8}.

In the spatial discretization, the first- and second-order derivatives in equations (6)-(9), except for convective terms, were discretized using central differencing which are fourth-order accurate. The following fourth-order scheme, where f denotes a dependant variable in the transformed regular coordinates, is used,

$$\frac{\partial f}{\partial \xi} = \frac{4}{3}\left[\frac{f_{i+1,j,k} - f_{i-1,j,k}}{2\Delta\xi}\right] - \frac{1}{3}\left[\frac{f_{i+2,j,k} - f_{i-2,j,k}}{4\Delta\xi}\right] \tag{18}$$

$$\frac{\partial^2 f}{\partial \xi^2} = \frac{16(f_{i+1,j,k} + f_{i-1,j,k}) - 30f_{i,j,k} - (f_{i+2,j,k} + f_{i-2,j,k})}{12\Delta\xi^2} \tag{19}$$

To avoid numerical instability, the convective terms are approximated using the fourth-order accurate upwind-biased differences (Rai and Moin, 1991). For example,

$$\frac{1}{J}\frac{\partial \psi}{\partial \eta}\frac{\partial \omega}{\partial \xi}$$

can be evaluated as

$$\left(u_1\frac{\partial \omega}{\partial \xi}\right)_{i,j} = (u_1)_{i,j}[-6(\omega)_{i+2,j} + 60(\omega)_{i+1,j} + 40(\omega)_{i,j} \tag{20}$$
$$- 120(\omega)_{i-1,j} + 30(\omega)_{i-2,j} - 4(\omega)_{i-3,j}]/(120\Delta\xi)$$

if

$$u_1 = \frac{1}{J}\frac{\partial \psi}{\partial \eta} > 0$$

and

$$\left(u_1 \frac{\partial \omega}{\partial \xi}\right)_{i,j} = (u_1)_{i,j}[4(\omega)_{i+3,j} - 30(\omega)_{i+2,j} + 120(\omega)_{i+1,j}$$

$$- 40(\omega)_{i,j} - 60(\omega)_{i-1,j} + 6(\omega)_{i-2,j}]/(120\Delta\xi)$$

(21)

if $u_1 < 0$.

In the time discretization, the following second-order accurate Adams-Bashforth method is used

$$f^{n+1} = f^n + \Delta t \left[\frac{3}{2}\left(\frac{\partial f}{\partial t}\right)^n - \frac{1}{2}\left(\frac{\partial f}{\partial t}\right)^{n-1}\right]$$

(22)

Test case and discussions

The numerical simulations described below were carried out on a Windows 98 PC platform with a 1.6 GHz Intel CPU and 256 MB RAM. Finer grids were introduced in the boundary layer regions. Because of the complexity of the flow patterns, finer grids are sometimes required to be arranged in other regions. Self-adaptive grid generation methods have been used to cope with this situation. This will be reported in a future paper.

Natural convection between eccentric cylinders

Figure 1 shows the general eccentric configuration of two circular cylinders of diameters D_o and D_i with vertical and horizontal eccentricities ε_V and ε_H, and with eccentric angle α. The flow in the annular space is laminar with no-slip conditions. On solid boundaries, equations (2) and (3) can be written as

$$\frac{\partial p}{\partial x} = \Pr \frac{\partial}{\partial y}(\nabla^2 \psi)$$

(23)

$$\frac{\partial p}{\partial y} = -\Pr \frac{\partial}{\partial x}(\nabla^2 \psi) + \Pr R_T T$$

(24)

The condition for a single value pressure field is (Thompson *et al.*, 1974),

$$\oint_l \nabla p \, d\vec{r} = 0$$

where l can be any closed curve in the flow field. Therefore, along the outer cylinder boundary, we have
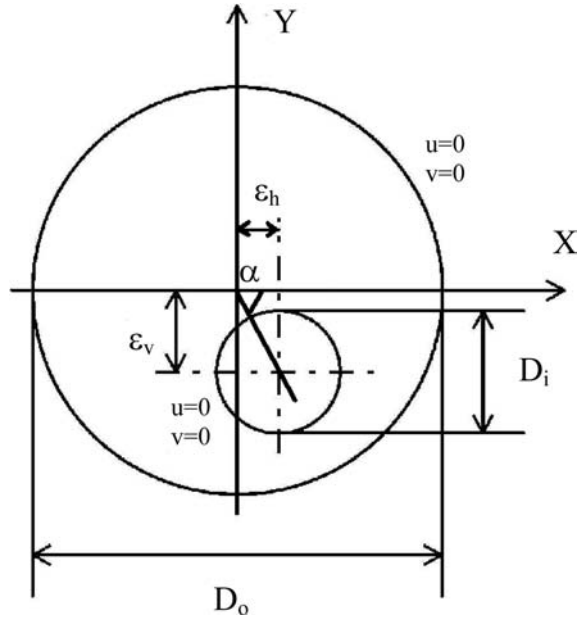
Figure 1.
Geometry of annulus

$$-\oint_l \left(\frac{\partial}{\partial y} (\nabla^2 \psi) \sin \alpha + \frac{\partial}{\partial x} (\nabla^2 \psi) \cos \alpha - R_T T \cos \alpha \right) \Pr \, dl$$

$$= -\Pr \oint_l \frac{\partial}{\partial n} (\nabla^2 \psi) \, dl = 0 \tag{25}$$

where $\vec{n} = (\cos \alpha, \sin \alpha)$ is the unit vector in the normal direction.

Because we have arranged normal coordinate lines in the vicinity of the cylinders, equation (25) becomes

$$\oint_l \frac{\partial \omega}{\partial \eta} \, dl = 0 \tag{26}$$

Using fourth-order difference formula on the outer cylinder ($j = 1$), we have

$$\oint_l \left(4\omega_2 - 3\omega_3 + \frac{4}{3} \omega_4 - \frac{1}{4} \omega_5 - \frac{25}{12} \omega_o \right) \Big/ \Delta \eta \, dl = 0 \tag{27}$$

in which

$$\omega_o = \omega_{\text{outer cylinder}} = \omega_{j=1} = -\frac{\partial^2 \psi}{\partial \eta^2}\bigg|_{j=1}$$

$$= -\frac{108\psi_2 - 27\psi_3 + 4\psi_4 - 85\psi_o}{18\Delta\eta} + O(\Delta\eta^3) \tag{28}$$

From equations (27) and (28), the value of the stream function on the outer cylinder can be obtained. The value on the inner cylinder is zero.

For this study, temperature boundary conditions are written as follows:

- $T_o = 0$ on wall of outer cylinder
- $T_i = 1$ on wall of inner cylinder

The simulation of natural convection in a concentric annulus was selected to verify our method (Figure 2(a)). The computed values of average equivalent conductivities were used to compare the present results with the available data in the work of Kuehn and Goldstein (1978) and Shu and Wu (2002). The average equivalent conductivities are defined as

$$\bar{k}_{\text{eqi}} = -\frac{\ln(rr)}{2\pi(rr-1)} \int_0^{2\pi} \frac{\partial T}{\partial r} \, \mathrm{d}\theta \tag{29}$$

for the inner cylinder, and

$$\bar{k}_{\text{eqo}} = -\frac{rr\ln(rr)}{2\pi(rr-1)} \int_0^{2\pi} \frac{\partial T}{\partial r} \, \mathrm{d}\theta \tag{30}$$

for the outer cylinder.

The computed values of average equivalent conductivities for the case of $rr = D_i/D_o = 2.6$ and $L/D_i = 0.8$ are compared with the results of Kuehn and Goldstein (1978) and Shu and Wu (2002), where $L = (D_o - D_i)/2$ is the difference of the two radii. Table I shows the comparison of average equivalent conductivities for the concentric configuration for four different values of the Rayleigh number, 10^2, 10^3, 10^4 and 5×10^4. The mesh sizes used in the this paper are 151×31 and time step $\Delta t = 5 \times 10^{-6}$. Numerical results agree very well with the previous results.

To further test the proposed method, numerical calculations were performed for various configurations of ε/L. The boundary-fitted coordinate systems for $\varepsilon_V/L = -0.623$ and $\varepsilon_V/L = 0.652$ with $rr = 2.6$, and $\varepsilon_h/L = 0.25$, 0.5 and 0.75 with $rr = 2.36$ are shown in Figure 2(b)-(g). The coordinate lines that intersect the walls are arranged perpendicular to the walls (Li et al., 1998), Therefore,
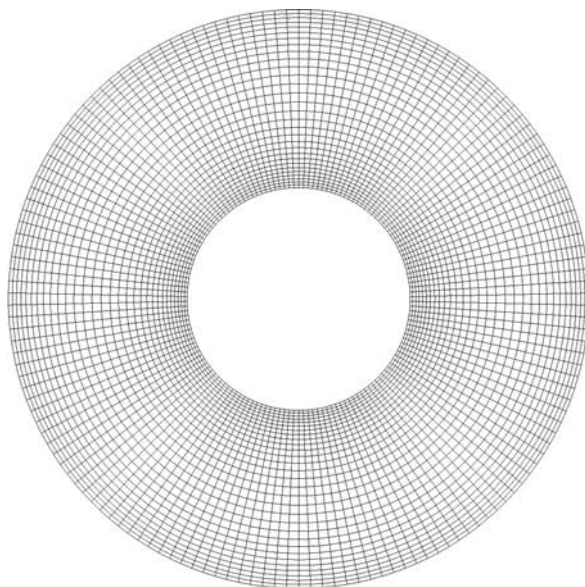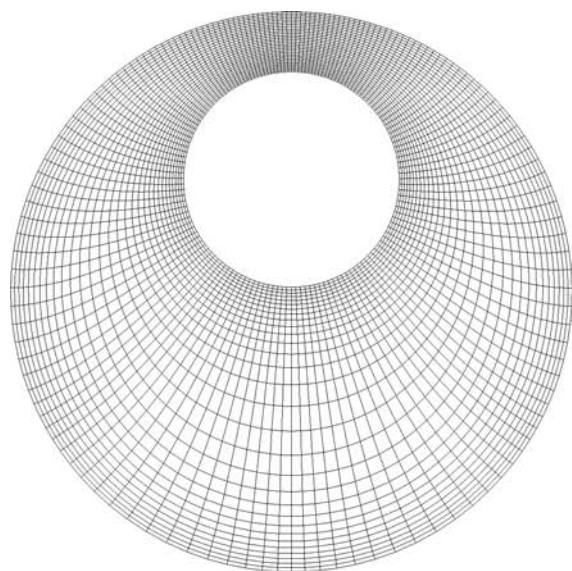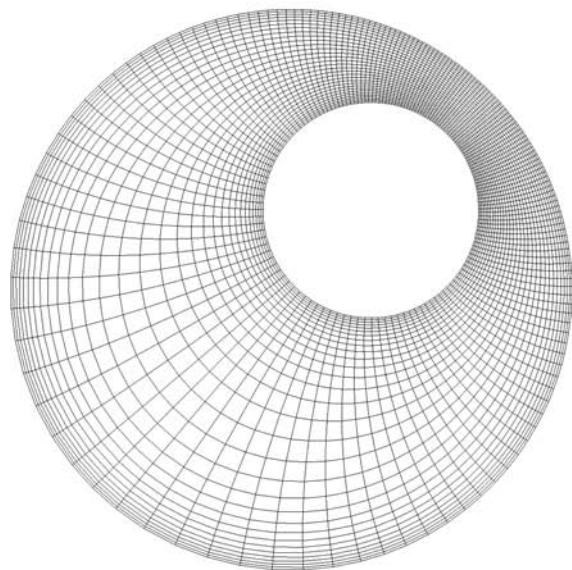
(a) for concentric cylinders
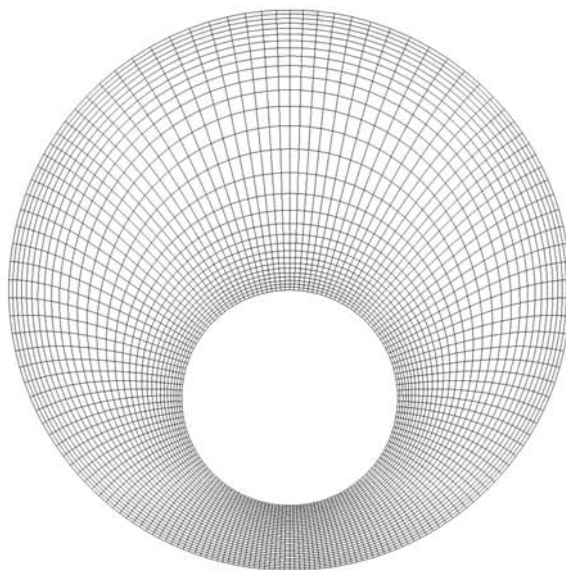
(b) $\varepsilon_V / L = -0.623$

Figure 2.
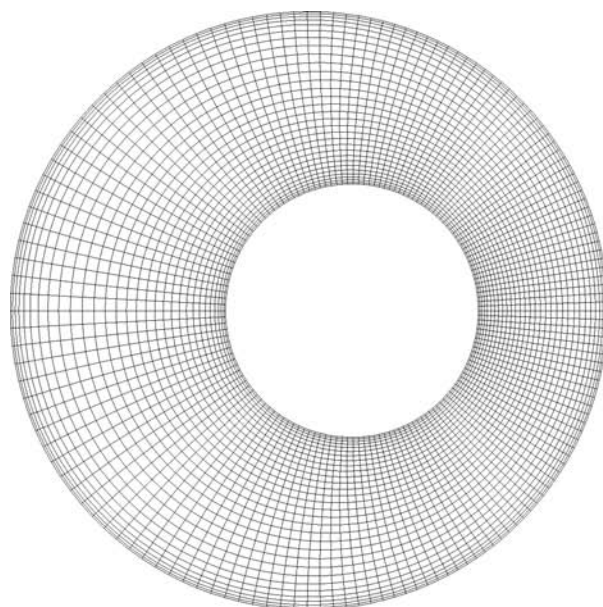Boundary-fitted
coordinate system for
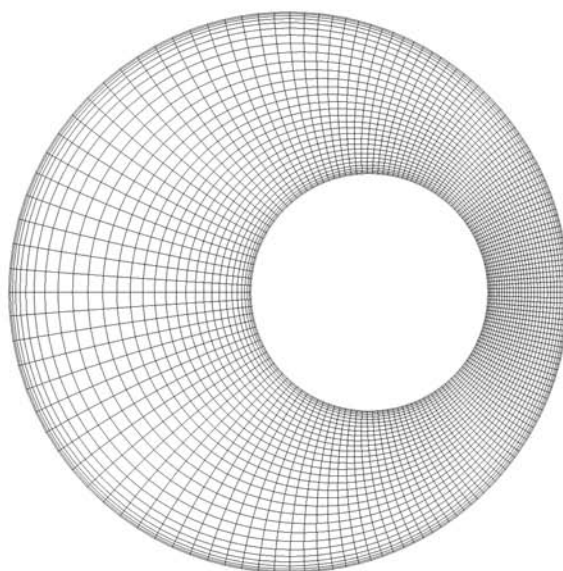annular cylinders

(c) $\varepsilon_V / L = 0.652$

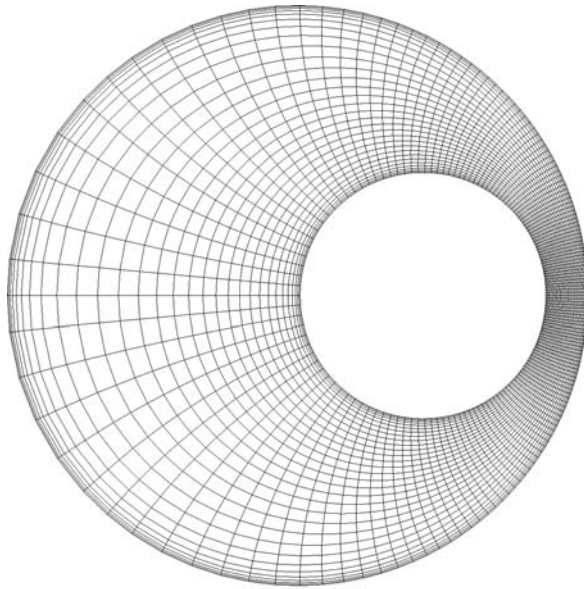(d) $\varepsilon = 0.652, \alpha = 45^0$

(Continued)

Figure 2.

(e) $\varepsilon_h / L = 0.25$

(f) $\varepsilon_h / L = 0.5$

Figure 2.

(g) $\varepsilon_h / L = 0.75$

Figure 2.

| Ra | $\bar{k}_{eqi}$ (Inner cylinder) | | | $\bar{k}_{eqo}$ (Outer cylinder) | | |
	Present study	Shu and Wu	Kuehn and Goldstein	Present study	Shu and Wu	Kuehn and Goldstein
10^2	1.005	1.001	1.000	1.000	1.001	1.002
10^3	1.089	1.082	1.081	1.084	1.082	1.084
10^4	2.000	1.976	2.010	1.994	1.976	2.005
5×10^4	2.995	2.953	3.024	2.997	2.952	2.973

$$\frac{\partial T}{\partial r} = \frac{\partial T}{\partial \eta} \bigg/ \frac{\partial r}{\partial \eta}$$

on the walls and it is convenient to calculate the local equivalent conductivities. For cases with only vertical eccentricity, numerical and experimental results of the local equivalent conductivities are shown in Figure 3. For $\varepsilon_V / L = -0.623$, the flow is steady and numerical results agree well with the experimental data. However, for $\varepsilon_V / L = 0.652$, periodic flow state occurs in the region near $\delta = 0$ and the period is about 3. Initially, the flow is symmetric and two symmetric cells occur at $t = 0.5$ near $\delta = 0$ (Figure 4(a)) and the local equivalent conductivity on the outer cylinder is small (Figure 4(b)). Gradually, the
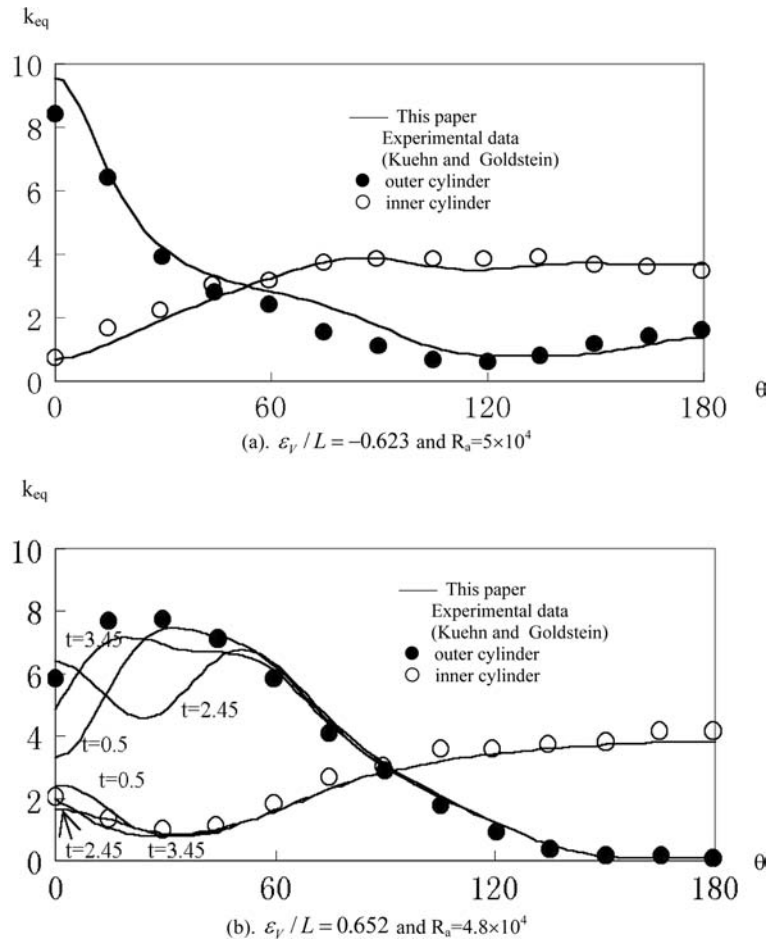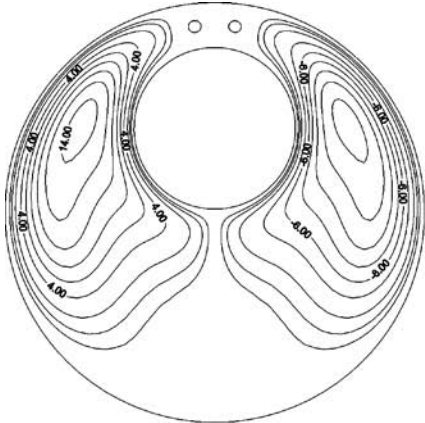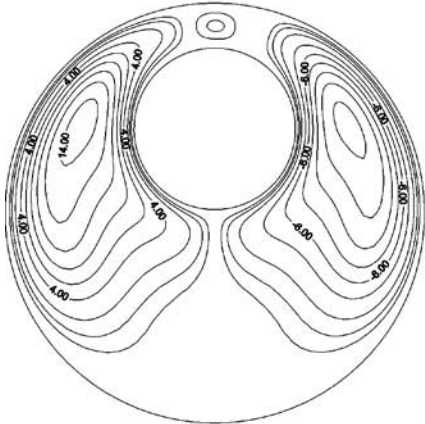
Figure 3.
Comparison of eccentric
local heat transfer
coefficients

symmetric state is broken and two secondary cells mix and merge to become
one cell at $t = 1.95$ (Figure 4(b)). At this stage, the heat transfer rate at the top
of the cylinder increases. The secondary cell rotates clockwise and mixes with
the right vortex (Figure 4(c)). Again the flow is symmetric and two symmetric
cells exist. At about $t = 3.45$ one secondary cell occurs again, but this time it is
anti-clockwise. At $t = 4.95$, the flow pattern is nearly the same as that at
$t = 1.95$. Basically, the numerical results are consistent with the experimental
data. The periodic phenomenon cannot be reflected in the experimental data of
Kuehn and Goldstein (1978). However, a similar phenomenon is observed in the
experiment of Labonia and Guj (1998). The authors opine that the experiment
data of Kuehn and Goldstein (1978) represent only the maximum local
equivalent conductivity at each point on the outer cylinder. The oscillation
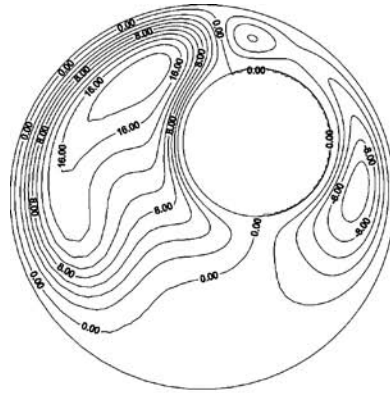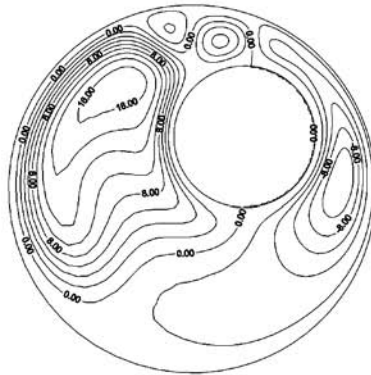
(a) at t=0.5

(b) at t=1.95
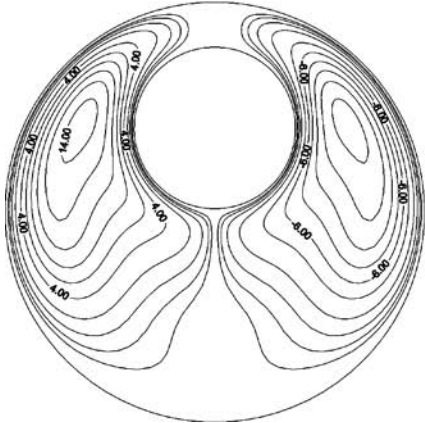
(c) at t=2.5

Figure 4.
Stream lines for
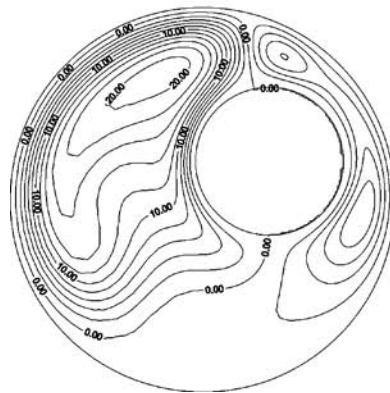$\varepsilon_V/L = 0.652$

phenomenon can be obtained not only for the vertical eccentric case, but also for cases with both vertical and horizontal eccentricities when $40° \leq \alpha \leq 130°$ (Figure 5(a) and (b)). When $\alpha \leq 39°$ or $\alpha \geq 131°$, the flow is steady. Figure 5(c) shows one of the steady cases with $\alpha = 30°$. Projahn *et al.* (1981) also used the

(a) Unsteady flow
    for α=45⁰ at t=2

(b) Unsteady flow
    for α=45⁰ at t=3

(c) Steady flow for α=30⁰

Figure 5.
Stream lines for cases with both vertical and horizontal eccentricities for $\varepsilon = 0.652$ and $rr = 2.6$ at $R_T = 4.8 \times 10^4$

same experimental data to verify their numerical analysis. The numerical results in this paper are more reasonable than those of Projahn et al. (1981).

For cases with only horizontal eccentricity when $rr = 2.36$, the present numerical results are shown in Table II and Figure 6. They agree well with the numerical results of Guj and Stella (1995) and Lee et al. (2002).

Symmetry breaking and overturning states in thermohaline-driven flows
Figure 7 shows the boundary-fitted coordinate system. The computational mesh consists of 81×51 grid points. The function $T_s(x)$ is given by

$$T_s(x) = \frac{1}{2}\left[\cos\left(2\pi\left(x - \frac{1}{2}\right)\right) + 1\right] \tag{31}$$

and flux $Q_s(x)$ through the top boundary is the same as that in Dijkstra and Molemaker (1997). It is chosen such that the integral over the surface is zero, that is

$$\frac{\partial S}{\partial y} = \delta Q_s(x) = \delta\left(3\cos\left(\beta\pi\left(x - \frac{1}{2}\right)\right) - \frac{6}{\beta\pi}\sin\left(\beta\frac{\pi}{2}\right)\right) \tag{32}$$

The parameter δ is a measure of the strength of the surface salt-flux and $Q_s(x)$ defines the spatial variation, which can also be changed by varying the value of β.

In our computation, the parameters $\beta = 2.6$, $R_T = 5 \times 10^6$ and time step $\Delta t = 5 \times 10^{-7}$. The parameters $Pr = 2.25$, $Le = 1$ are fixed as in Dijkstra and Molemaker (1997) and Quon and Ghil (1992). The values of Pr and Le are chosen for comparison with their results. To obtain the symmetric breaking flow pattern, perturbations of salinity are introduced on the first horizontal grid line next to the top boundary in the left side of the cavity at the beginning of the computation. The perturbations are as follows:

$$S' = 5 \times 10^{-4}\left|\sin\left(2\pi\left(\frac{t}{100\Delta t} - x\right)\right)\right| \quad 0.0015 \le t < 0.002 \tag{33}$$

and

| $\frac{\varepsilon_h}{L}$	R_T	ψ_{max}			$|\psi_o|$		
		Present	Guj et al.	Lee et al.	Present	Guj et al.	Lee et al.
0.0	5.3×10^3	9.42	9.23	9.075	0.0	0.0	0.00
	4.59×10^4	24.56	26.03	24.66	0.0	0.0	0.00
0.25	5.3×10^3	12.06	12.47	11.66	0.251	0.225	0.284
	4.59×10^4	24.74	27.97	24.67	1.750	1.694	1.872
0.5	5.3×10^3	13.17	14.27	12.96	0.546	0.576	0.645
	4.59×10^4	24.97	28.91	24.59	2.622	2.790	3.047
0.75	5.3×10^3	13.92	15.37	13.67	0.617	0.624	0.744
	4.59×10^4	25.11	28.04	24.73	2.867	3.186	3.410

Table II.
Comparison of values of
the stream function for
horizontal eccentric
cases
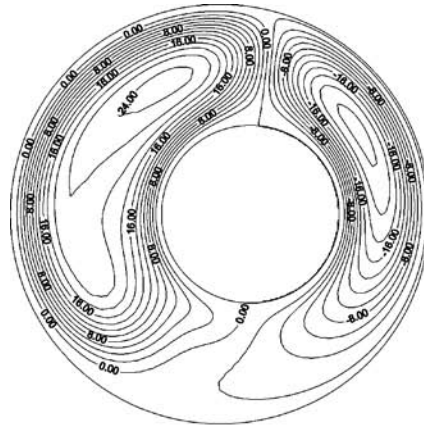
(a) $\varepsilon_h/L = 0.25$
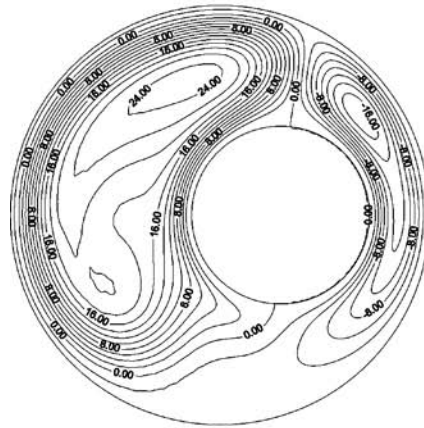
(b) $\varepsilon_h/L = 0.5$
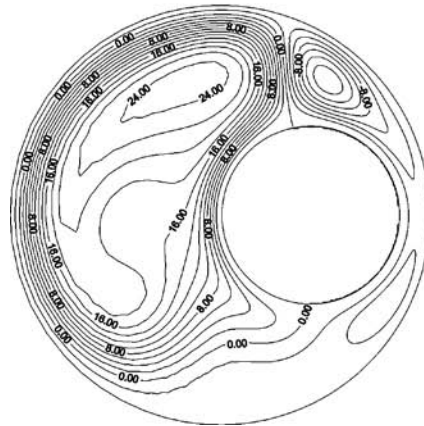
(c) $\varepsilon_h/L = 0.75$

Figure 6.
Stream lines for different
values of ε_h/L at
$R_T = 4.59 \times 10^4$

$$S' = -5 \times 10^{-4} \left| \sin\left(2\pi\left(\frac{t}{100\Delta t} - x\right)\right)\right| \quad 0.0035 \le t < 0.004 \qquad (34)$$

When the salt-flux condition is applied while the symmetric state is perturbed, the perturbed particles will gain speed. This continuous increase in speed will cause instability. When δ is small, the symmetry state cannot be broken (Figure 8). As δ increases, the asymmetry state and overturning state can be obtained as shown in Figures 9 and 10. The same phenomena can be observed in Figure 5 of Dijkstra and Molemaker (1997), and Figure 9 of Quon and Ghil
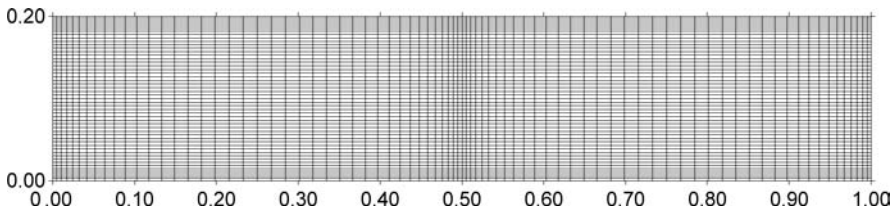

Figure 7.
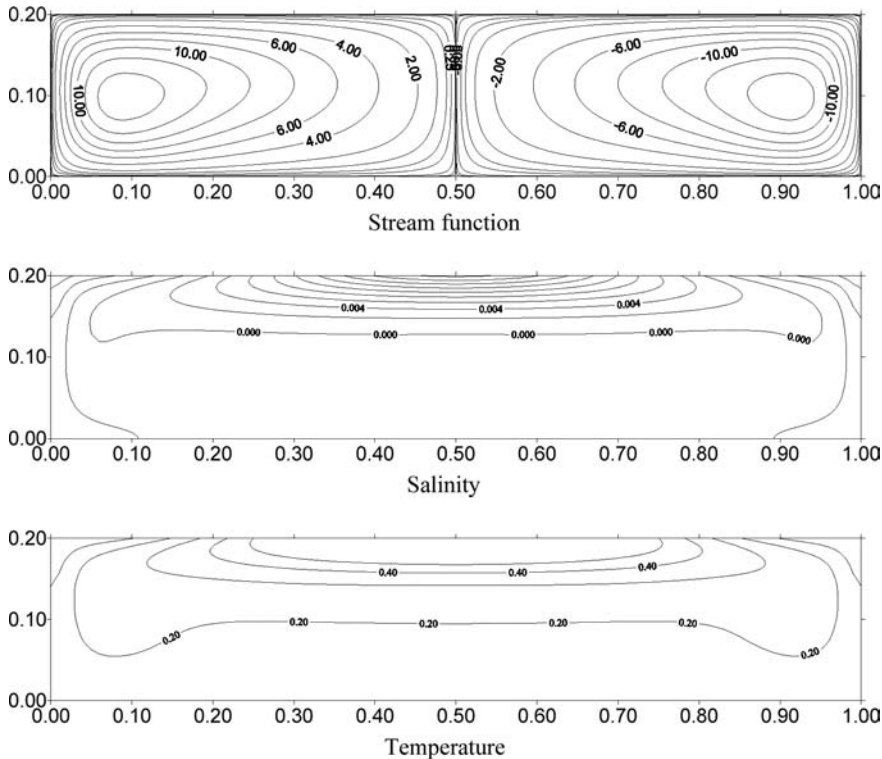Transformed grid with improved resolution at boundary layer regions

Stream function

Salinity

Temperature

Figure 8.
Symmetry state at
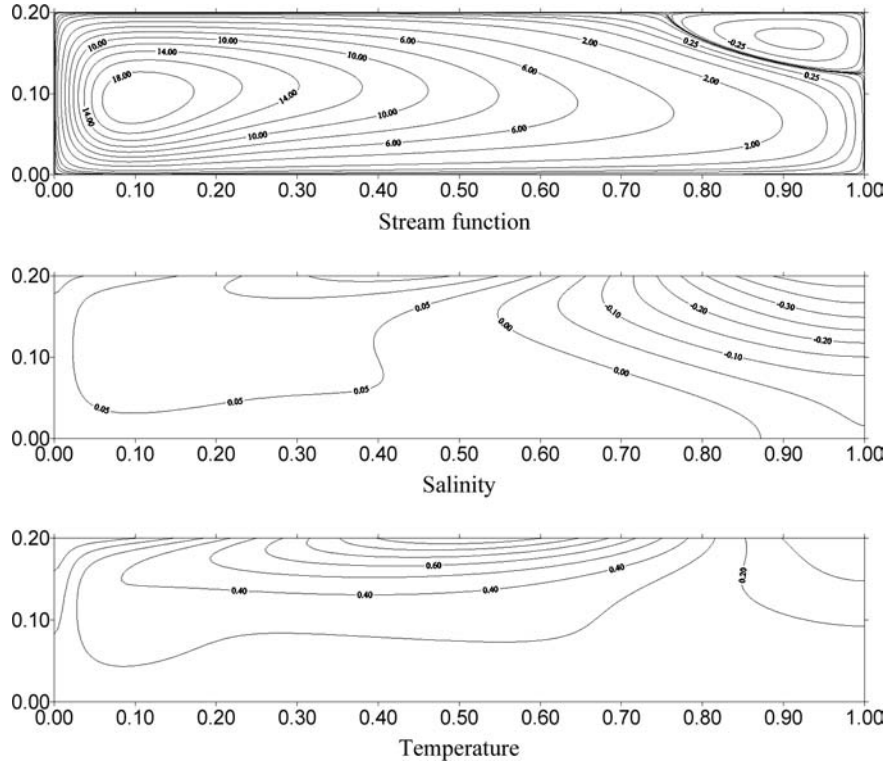$t = 0.3$ with $\delta = 0.25$

Figure 9.
Asymmetry state at
$t = 0.3$ with $\delta = 3$

(1992). The numerical results agree well with their results. This test case is only used to verify the proposed numerical method. The effect of the magnitude of the Rayleigh numbers and the strength of the salinity flux on the physical mechanism of pitchfork bifurcation from symmetric to asymmetric states has been studied systematically by Quon and Ghil (1992). The physics of the transitions and the detailed bifurcation structure of the thermohaline-driven flows have been obtained by Dijkstra and Molemaker (1997) using the path-following techniques. The details are not repeated here.

Periodic oscillatory phenomenon under neutral buoyancy
The same convection problem was studied again, but with the buoyancy ratio $R_\rho = 1$ and Prandtl number, $\text{Pr} = 1$. The salinity profile at the top boundary is now specified, using the same profile as the temperature defined by equation (31). The time variations of the kinetic energy of the system defined is shown in Figure 11.
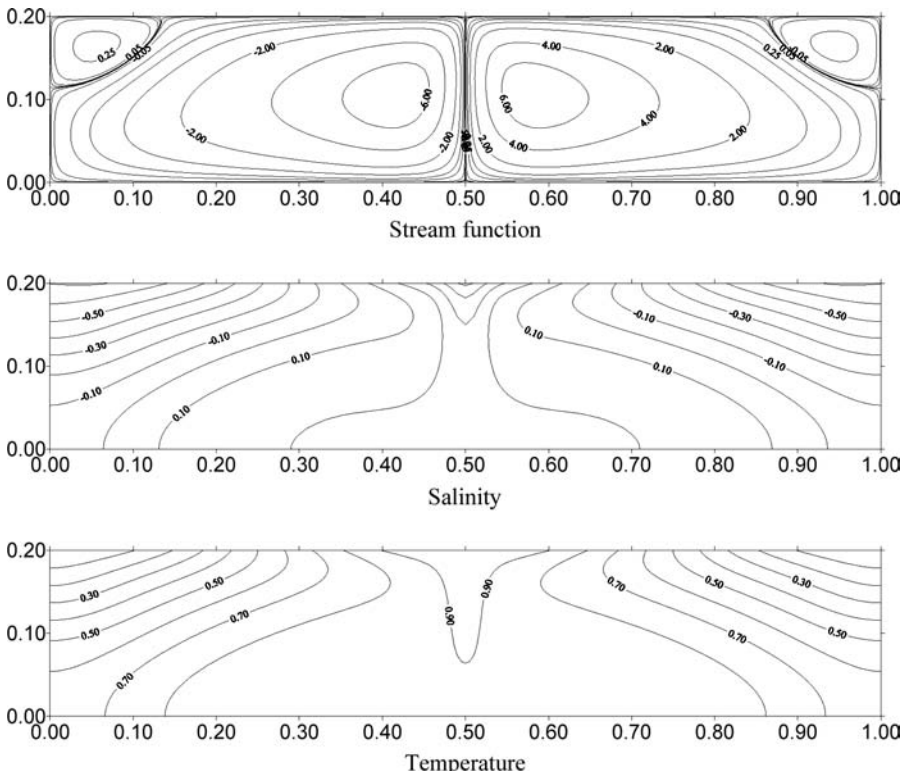
$$E_m = \frac{1}{A} \int_A \int \frac{1}{2}(u^2 + v^2)\,\mathrm{d}x\,\mathrm{d}y \qquad (35)$$

where A is the area of the computational domain and u and v are the two velocity components. The no-slip boundary conditions are used in the vertical sidewalls and bottom boundary.

It can be seen from Figure 11 that the flow field is oscillatory when Le < 1. The period of the oscillations decreases with increasing values of Le. The period is 0.099, 0.051, 0.043 and 0.036 when Le = 0.9, 0.8, 0.7 and 0.6, respectively. Also the motion becomes progressively more vigorous, with a corresponding increase in randomness as the period shortens. The unsteadiness can be clearly seen in Figure 11 when Le ≤ 0.8. When Le is large, the flow again becomes unsteady. When Le = 4, the flow is already highly unsteady. Randomness occurs with further increase in Le as exemplified by the case Le = 10. The occurrence of oscillations is the cause of flow instability. Because of density differences, warm and less saline water tends to rise to the surface in the case of ocean flow; while cold and more saline water tends to sink to the bottom. However, the surface seawater in the two polar regions are cold and less saline in the case of ocean flow; while that at the equator is warm and more saline relative to the bottom seawater. The opposing effects of temperature and salinity lead to the oscillatory circulations in the
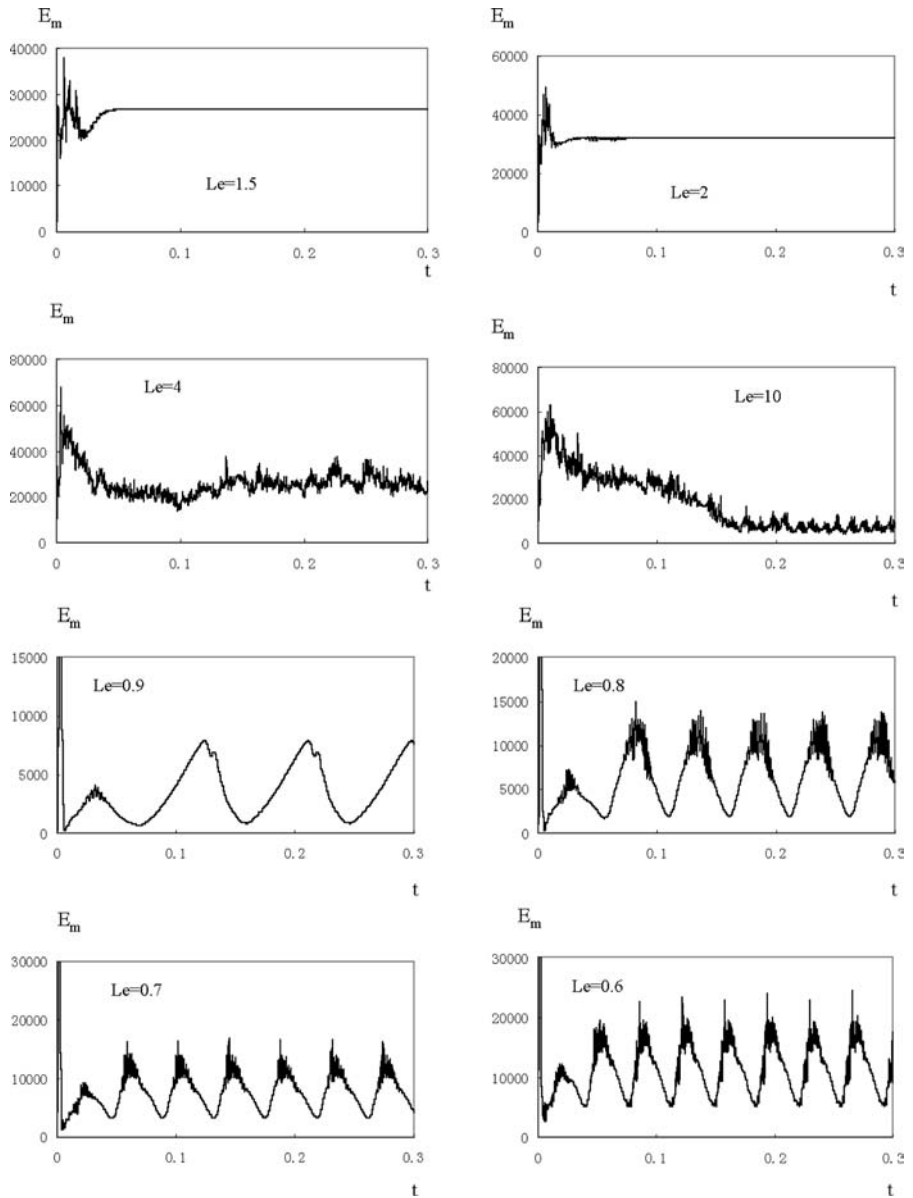
Figure 11.
Curves of average energy

oceans. Periodic oscillation is the intermediate state between the steady and random motions.

The time variation of the flow structure in one cycle of oscillation at $Le = 0.8$ is shown in Figure 12. The period in this case is 0.051. The flow and temperature fields at $t = 0.17, 0.18, 0.19, 0.20, 0.21$ and 0.22 were compared.

Stream function at t=0.17

Temperature at t=0.17

Stream function at t=0.18

Temperature at t=0.18

Stream function at t=0.19

Temperature at t=0.19

Stream function at t=0.20

Temperature at t=0.20

Stream function at t=0.21

Temperature at t=0.21
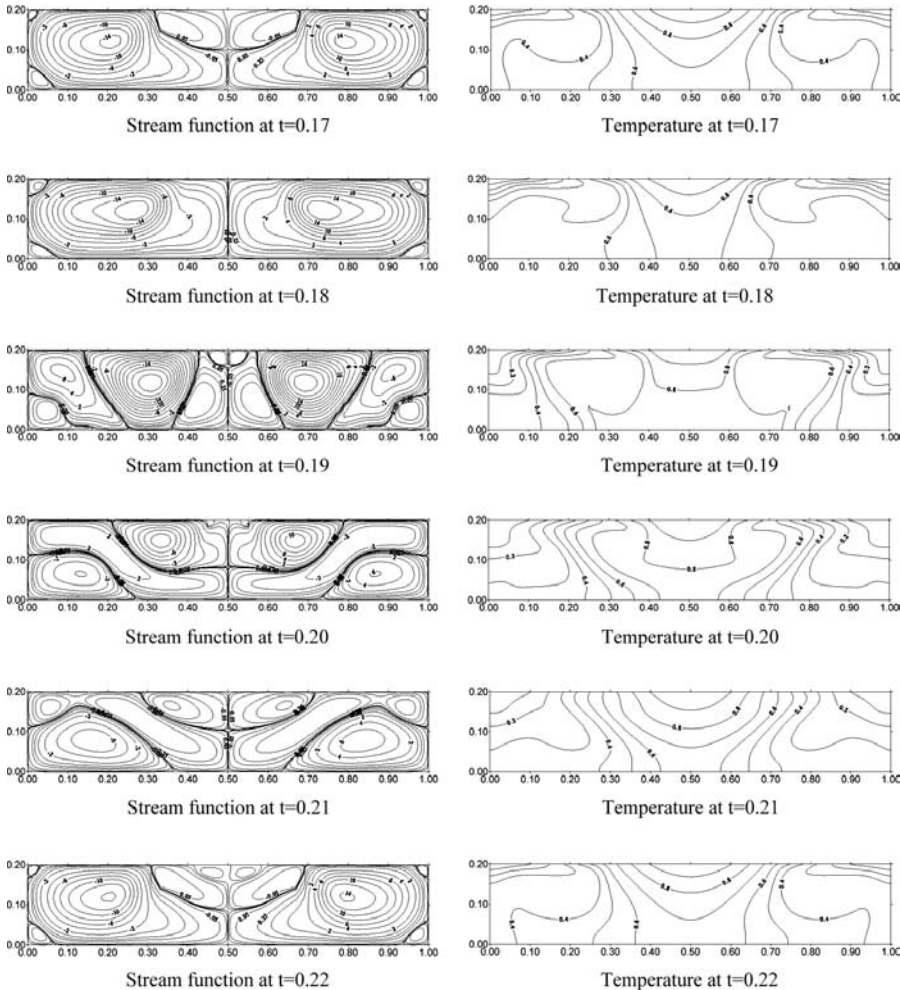
Stream function at t=0.22

Temperature at t=0.22

Figure 12.
Oscillation phenomena at
Le = 0.8

The basic structure is that the main eddy moves towards the centre of the cavity and secondary eddies are formed at the four corners. Because of the temperature and salinity boundary conditions imposed on the top surface, the two secondary eddies at the two top corners develop first and prevent the main eddy from contacting the two secondary eddies at the two bottom corners. With the development and strengthening of the two eddies at the top corners, the main eddy in the centre weakens and eventually disappears. The two secondary eddies at the bottom develop at the same time and merge to replace the disappearing main eddy. The temperature field is also oscillatory. The behaviour of the salinity field is similar to that of the temperature field and hence is not shown.

When Le < 1, multiple unstable eddies appear in the flow field. For example, when Le = 0.8, ten eddies appear at $t = 0.19$ as shown in Figure 12. When Le = 0.6, 14 eddies appear at $t = 0.196$ as shown in Figure 13. The steady motion when Le = 2 is shown in Figure 14. It can be seen that the main eddy on the left rotates in the anti-clockwise direction; while its counterpart on the right rotates in the opposite direction. As described earlier, randomness sets in with further increase in Le. For example, when Le = 4, the two main eddies are relatively stable. The secondary eddies rotate in the opposite direction and move towards the centre from the vertical sidewalls and the bottom (Figure 15). When Le = 10, the two main eddies are smaller while the secondary eddies become larger. The flow field is hence more unstable and less organized as shown in Figure 16.
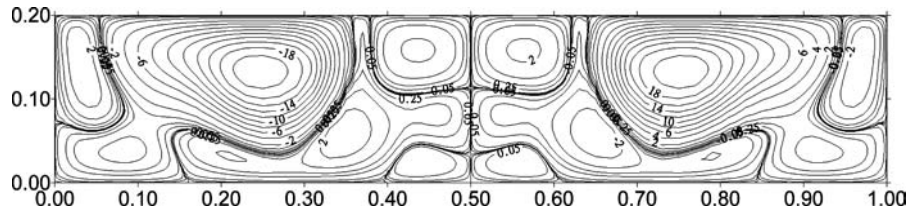

Figure 13.
Stream function at
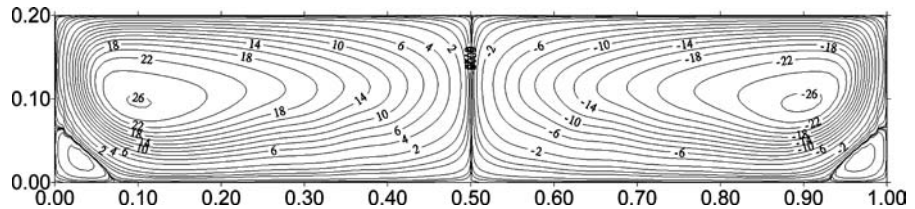$t = 0.196$ with Le = 0.6

Figure 14.
Stream function at
Le = 2.0

Figure 15.
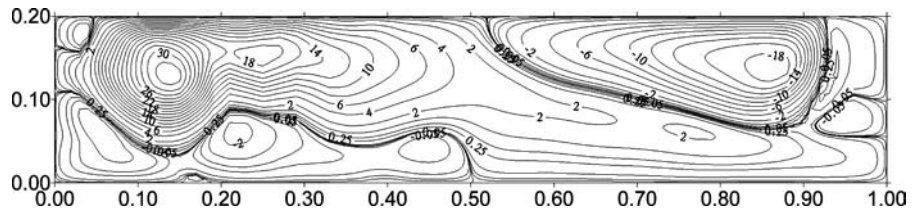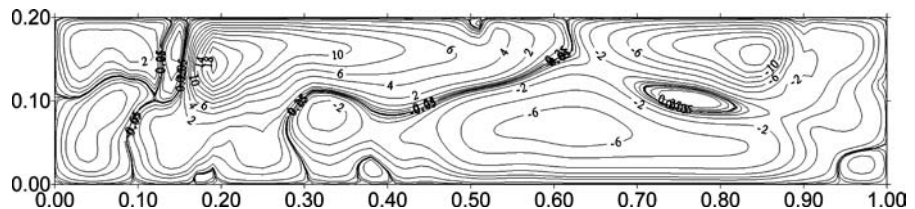Stream function at
$t = 0.15$ with Le = 4

Figure 16.
Stream function at
$t = 0.15$ with Le = 10

Conclusions

An accurate high-order difference method is proposed in this paper to solve double-diffusive problems using boundary fitted coordinate system so that improved resolution in the boundary layers can be achieved without excessive computational efforts. The system was first verified by simulating the natural convection between the eccentric cylinders to demonstrate the versatility of the boundary fitted coordinate system. The multiple equilibria in thermohaline flow in a rectangular cavity is then computed. Because the convection terms are approximated using fourth-order upwind differences, the numerical scheme has good stability characteristics. The numerical example shows that the complicated oscillatory motions of double-diffusive systems can be successfully modelled by the proposed method. When Le > 1, multiple eddies appear during the cycle of oscillation. When the average kinetic energy of the system is large, instability occurs. When Le is less than unity, the steady motion becomes progressively more unsteady as the value of Le decreases. The flow eventually becomes chaotic when Le is sufficiently small. The method proposed in this paper can be used to simulate various double-diffusive problems.

References

Chen, C.F., Briggs, D.G. and Wirtz, R.A. (1971), "Stability of thermal convection in a salinity gradient due to lateral heating", *Int. J. Heat Mass Transfer*, Vol. 14, pp. 57-65.

Dijkstra, H.A. and Molemaker, J.J. (1997), "Symmetry breaking and overturning states in thermohaline-driven flows", *J. Fluid Mech.*, Vol. 331, pp. 169-98.

Guj, G. and Stella, F. (1995), "Natural convection in horizontal eccentric annuli: numerical study", *Numerical Heat Transfer, Part A*, Vol. 27, pp. 89-105.

Heinrich, J.C. (1984), "A finite element model for double-diffusive convection", *Int. J. Numerical Methods Eng.*, Vol. 20, pp. 447-64.

Kuehn, T.H. and Goldstein, R.J. (1978), "An experimental study of natural convection in the concentric and eccentric horizontal cylindrical annuli", *ASME J. Heat Transfer*, Vol. 100, pp. 635-40.

Labonia, G. and Guj, G. (1998), "Natural convection in a horizontal concentric cylindrical annulus: oscillatory flow and transition to chaos", *J. Fluid Mech.*, Vol. 375, pp. 179-202.

Lee, J.W. and Hyun, J.M. (1990), "Double-diffusive convection in a rectangle with opposing horizontal temperature and concentration gradients", *Int. J. Heat Mass Transfer*, Vol. 33, pp. 1619-32.

Lee, J.W. and Hyun, J.M. (1991), "Time-dependent double diffusion in a stably stratified fluid under lateral heating", *Int. J. Heat Mass Transfer*, Vol. 34, pp. 2409-15.

Lee, T.S., Hu, G.S. and Shu, C. (2002), "Application of GDQ method for the study of natural convection in horizontal eccentric annuli", *Numerical Heat Transfer, Part A*, Vol. 41, pp. 803-15.

Li, Y.S., Zhan, J.M. and Sun, M.G. (1998), "Matching boundary-fitted grid generation to physical boundary conditions with applications to natural convection problems", *Numerical Heat Transfer, Part A*, Vol. 33, pp. 621-34.

Nishimura, T. and Kawamura, T. (1992), "Numerical errors of Galerkin finite-element method for natural convection of a fluid layer or a fluid-saturated porous layer", *Numerical Heat Transfer, Part A*, Vol. 22, pp. 241-55.

Nishimura, T. and Kunitsugu, K. (2000), "Direct numerical simulation of layer merging in a salt-stratified system", *Numerical Heat Transfer, Part A*, Vol. 37, pp. 323-41.

Projahn, U., Rieger, H. and Beer, H. (1981), "Numerical analysis of laminar natural convection between concentric and eccentric cylinders", *Numerical Heat Transfer*, Vol. 4, pp. 131-46.

Quon, C. and Ghil, M. (1992), "Multiple equilibria in thermosolutal convection due to salt-flux boundary conditions", *J. Fluid Mech.*, Vol. 245, pp. 449-84.

Quon, C. and Ghil, M. (1995), "Multiple equilibria and stable oscillations in thermosolutal convection at small aspect ratio", *J. Fluid Mech.*, Vol. 291, pp. 33-56.

Rai, M.M. and Moin, P. (1991), "Direct simulation of turbulent flow using finite-difference schemes", *J. Comput. Physics*, Vol. 96, pp. 15-53.

Shu, C. and Wu, Y.L. (2002), "Domain-free discretization method for doubly connected domain and its application to simulate natural convection in eccentric annuli", *Comput. Methods Appl. Mech. Eng.*, Vol. 191, pp. 1827-41.

Thompson, J.F. (1980), "Numerical solution of flow problems using body-fitted coordinate system", in Kollmann, W. (Ed.), *Computational Fluid Dynamics*, Hemisphere Publishing Corporation, New York, pp. 1-98.

Thompson, J.F., Thames, F.C. and Mastin, C.W. (1974), "Automatic numerical generation of body-fitted curvilinear coordinate system for fields containing any number of arbitrary two-dimensional bodies", *J. Comput. Phys.*, Vol. 15, pp. 299-319.